Design and Projected Performance of a Flapping Foil AUV

Stephen Licht, Victor Polidoro, Melissa Flores, Franz S. Hover, *Associate Member, IEEE*, and Michael S. Triantafyllou

Abstract—The design and construction of a biomimetic flapping foil autonomous underwater vehicle is detailed. The vehicle was designed as a proof of concept for the use of oscillating foils as the sole source of motive power for a cruising and hovering underwater vehicle. Primary vehicle design requirements included scalability and flexibility in terms of the number and placement of foils, so as to maximize experimental functionality. This goal was met by designing an independent self-contained module to house each foil, requiring only direct current power and a connection to the vehicle's Ethernet local area network for operation. The results of tests on the foil modules in the Massachusetts Institute of Technology (MIT) Marine Hydrodynamics Water Tunnel and the MIT Ship Model Testing Tank are both used to demonstrate fundamental properties of flapping foils and to predict the performance of the specific vehicle design based on the limits of the actuators. The maximum speed of the vehicle is estimated based on the limitations of the specific actuator and is shown to be a strong function of the vehicle drag coefficient. When using four foils, the maximum speed increases from 1 m/s with a vehicle C_D of 1.4 to 2 m/s when $C_D = 0.1$, where C_D is based on vehicle frontal area. Finally, issues of vehicle control are considered, including the decoupling of speed and pitch control using pitch-biased maneuvering and the tradeoff between actuator bandwidth and authority during both the cruising and hovering operation.

Index Terms—Biomimetic propulsion, flapping foils, underwater vehicles.

I. INTRODUCTION

THE PHYSICS of swimming and flying has been the focus of considerable theoretical, numerical, and experimental work. Examples of experimental work with live fish include [1]–[3] and biorobotic devices modeled on the blue-fin tuna [4], [5] and small-mouth bass [6] have been studied. One of the motivations has been to improve the design and performance of underwater vehicles, recognizing that in many ways there is an extraordinary gap between the abilities of man-made machines and those of fish and other marine animals. Quantitative comparisons between the hydrodynamics of fish and small underwater vehicles have been formulated, e.g., in [7]. Existing autonomous underwater vehicles (AUVs) are typically optimized primarily for high cruising efficiency with propellers and conventional lifting surfaces and, as a result are unsuited for use in confined spaces, at low speeds, near the surface, and in unsteady flow, conditions in which fish can thrive. A robust vehicle that exploits the hydrodynamics of fishlike swimming could yield impressive gains in maneuvering and hovering capabilities while maintaining the ability to cruise from station to station with high efficiency. Such a vehicle could serve as an extremely powerful tool in a wide range of applications.

The biomimetic flapping foil autonomous underwater vehicle (BFFAUV) was conceived as a test platform and proof of concept for the use of flapping foils as the sole source of propulsion and maneuvering forces in an underwater vehicle.

Extensive testing of oscillating foils has been performed in the Massachusetts Institute of Technology (MIT) Ship Model Testing Tank, resulting in a solid understanding of the fundamental parameters of thrust production in foils [8]–[10]. The BFFAUV represents our first attempt to tackle the issues involved in putting this knowledge into practice on a working vehicle scaled to support a significant scientific payload. The focus of our design has been on those issues that are related specifically to the foils themselves and the vehicle size, shape, and control systems were designed to be as flexible as possible.

II. VEHICLE REQUIREMENTS

The performance goals for the vehicle include a desired top speed of 2 m/s and sufficient maneuvering authority to independently control position in pitch, heave, surge, and sway. The functional requirements include the following:

- foil-based actuation—the primary goal of the program is to investigate the use of foils for propulsion and maneuvering;
- scalability and flexibility—freedom to adjust the foil actuator numbers, positions, and orientations will allow insights into the tradeoffs between different vehicle layouts and the corresponding control strategies;
- size constraints—2 m × 0.5 m × 0.5 m maximum dimensions for ease of deployment;
- autonomous operation—preprogrammed mission following, independent error handing, onboard power source, and data storage capability;
- shallow (10-m) confined water operation—a greater depth rating adds cost and complexity with no corresponding increase in experimental functionality;
- inertial navigation—minimal long-term tracking accuracy is required for short supervised missions focused on local control issues.
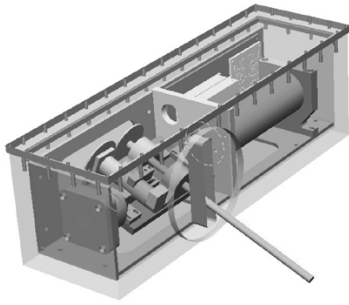
S. Licht, M. Flores, F. S. Hover, and M. S. Triantafyllou are with the Department of Ocean Engineering, Massachusetts Institute of Technology, Cambridge, MA 02139 USA (e-mail: slicht@mit.edu; mharness@mit.edu; hover@mit.edu; mistetri@mit.edu).

V. Polidoro is with Autonomous Underwater Vehicles Laboratory, Massachusetts Institute of Technology Sea Grant, Cambridge, MA 02139 USA (e-mail: polidoro@mit.edu).

Digital Object Identifier 10.1109/JOE.2004.833126

Fig. 1.   Single-housing actuator design.

III. VEHICLE DESIGN

A. Foil Actuators

The focus of much of the design effort for the vehicle was concentrated on the distinguishing characteristic of the vehicle: the foil actuation. A key requirement for the vehicle is scalability and flexibility in terms of the number of foils, as well as their positions and orientations. To meet the flexibility requirement, each foil actuator was conceived as part of a waterproof module that could be mounted anywhere on the vehicle frame and could be operated independently from the other foils. To allow for scalability, the modules are designed such that as more modules are added to the vehicle, there is no complexity added to the power and communication circuits.

A single foil module contains all the components necessary to add another foil to the vehicle. Each module contains a 190- and 15-W direct current (dc) brush motor with optical encoders (Litton-Polyscientific, Blacksburg, VA), which actuate foil roll and pitch, respectively. The corresponding motor control circuit is also housed in the module, with an Ethernet-enabled two-axis motion control card and two pulsewidth modulation (PWM) amplifiers. The addition of a new module entails only two connections: an Ethernet line to a central hub on the vehicle local area network (LAN) and a fused connection to the power bus. Since the hub acts in some sense like a bus connection, no additional wiring is required.

There are two generations of foil actuator designs. In the first design, all the components are placed in a single housing, as drawn in Fig. 1. While the mechanical actuation and internal wiring are straightforward within the single housing, the sealing is complex. The dynamic seal between the foil and housing limits the depth of operation, range of motion, and the fatigue lifetime. The first prototype was installed in the MIT Propeller Testing Tunnel for experiments as described later. A second iteration was then proposed to increase the depth rating of the actuator and the range of roll motion of the foil.

The second iteration of the design, which is currently installed on the vehicle, contains the same electrical components in two independently sealed cylindrical housings, as shown in Fig. 2. One cylinder remains stationary with respect to the vehicle and the second smaller cylinder rotates about its axis with respect to the larger. The use of two independently rotating housings simplifies the sealing problem, which improves the robustness of the seals. In addition, the full range of motion on the roll axis is improved to 180°, while the pitch motion remains completely unrestricted.
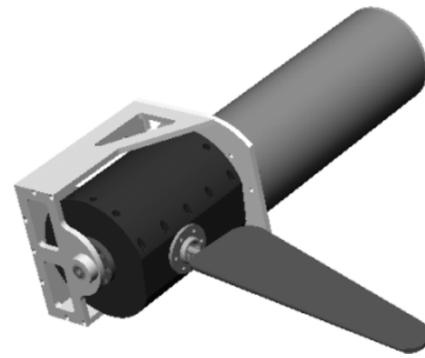

Fig. 2.   Dual-housing actuator design.

B. Electrical Systems and Communication

The power system is run at 24-V dc for reasons of safety and convenience, supplied by a pair of sealed lead acid (SLA) gel secondary cells connected in series. Actuator power cutoff, processor reset and power cycling, and total vehicle power kill switches are activated with magnetic proximity switches.

The central processor is an Octagon Systems Pentium III single-board computer running RedHat Linux v7.2, while each actuator module contains a Galil 1425 two-axis motion-control processor. A Crossbow six-axis accelerometer is used for navigation, with data collection performed by a 16-channel/12-bit 330-kHz analog-to-digital (A/D) converter from Eagle Technology (Cape Town, South Africa).

Each of the separate housings that comprise the vehicle are connected to an Ethernet LAN with a star-shaped topology centered on a housing containing a wireless access point and hub. The appeal of Ethernet lies in both high communication rates and the ease with which new components can be connected. The Galil motion-control cards were chosen in part for their compatibility with Ethernet communication; power distribution is controlled entirely through commands to an embedded server with digital input–output (I/O) capabilities (a Hello!Device 1100, Sena Technologies, Seoul, Korea). One result of the system architecture is that any computer running a web browser and the supplied software for the motion control card can route power to one or more foil modules and control the foil motion directly. Communication with the vehicle will only be possible while the vehicle is at the surface.

C. Primary Vehicle Layout Options

The two primary layouts envisioned for the vehicle involve four foils, placed so as to take advantage of port–starboard and top–bottom symmetry. The first consists of two pairs of foils placed port–starboard along the median line, at bow and stern, as drawn in two views in Fig. 3. (This configuration additionally results in fore–aft symmetry.) The second option shifts one pair of the foils 90° about the vehicle primary axis, so that they are oriented up–down, a configuration not unlike that adopted by the boxfish.

The primary advantage of maximizing symmetries is the resulting simplification of the control problem. The motion of the foils can be properly phased with respect to one another so as to cancel the unwanted cyclic forces that oscillating foils generally produce perpendicular to the desire impulse.
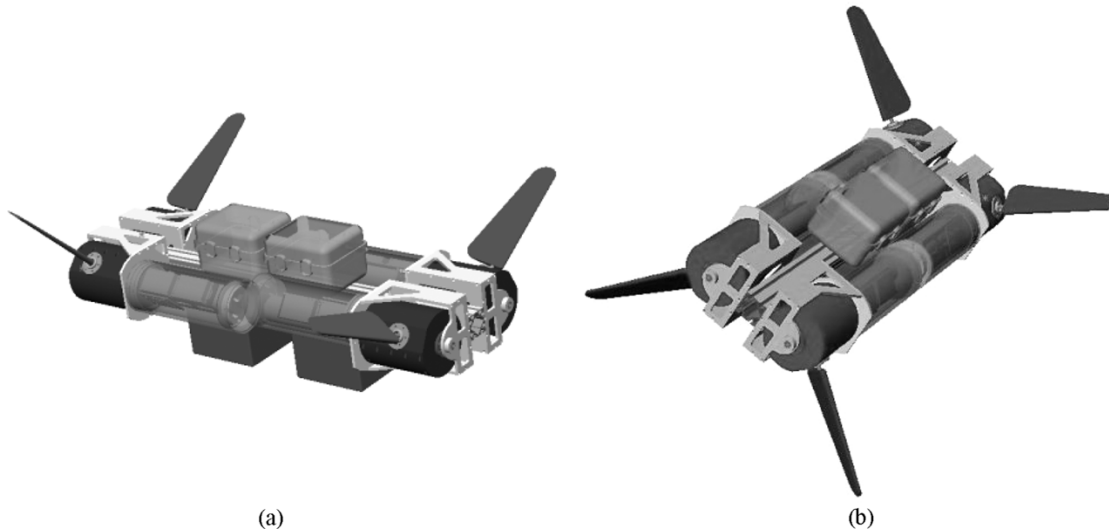
(a)

(b)

Fig. 3. Two views of fore–aft paired fin layout.

Initially, the vehicle is being assembled in the paired fore–aft fin arrangement. Maximum dimensions without foils are 2 m × 0.5 m × 0.5 m, while the foils protrude 0.4 m from each side, with 0.1-m average chord. All foils have a 180° range of motion in roll and unrestricted motion in pitch. The actuators are mounted to an aluminum spine that measures 5 cm × 10 cm with a rectangular cross section. All other vehicle components, including battery and electronics housings and foam for buoyancy, will be mounted directly to the same spine.

IV. ACTUATOR TESTING

The first and second iterations of foil modules designed for the vehicle were instrumented and tested in the MIT Hydrodynamics Laboratory and the MIT Ship Model Testing Tank, respectively. Measurements were made of thrust forces, lift forces, and power consumption.

The initial goal of the testing program was to assess the likely performance of the vehicle in three specific instances: high-speed cruising, transient maneuvering at speed, and hovering or station keeping.

A. Kinematics

The large displacement flapping motion of the wing is referred to as the roll motion. The twisting or feathering of the wing is referred to as the pitch motion. The basic motion tested involves sinusoidal roll-and-pitch motions, often referred to as "simple harmonic" foil kinematics.

The roll position of the foil is defined as

$$\phi(t) = \phi_0 \sin(\omega t) + \phi_{\text{bias}} \tag{1}$$

where ϕ_0 is the roll amplitude in radians and ω is the frequency of the foil motion in radians per second. ϕ_{bias} is a static roll bias used to change the mean roll position of the foil. For the purpose of testing with a single foil, ϕ_{bias} is arbitrary, but when multiple foils are in use on a vehicle, the absolute and relative values of ϕ_{bias} for the different foils comes into play as part of any control strategy.

The pitch position of the foil is defined as

$$\theta(t) = \theta_0 \sin(\omega t + \psi) + \theta_{\text{bias}} \tag{2}$$

where θ_0 is the pitch amplitude in radians and ψ is the phase angle between pitch and roll in radians. θ_{bias} is a static pitch bias used for maneuvering. The phase angle ψ, for all experiments described herein, is $\pi/2$; therefore, we can write $\theta(t)$ as

$$\theta(t) = \theta_0 \cos(\omega t) + \theta_{\text{bias}}. \tag{3}$$

For heaving and pitching foils, the motion is nondimensionalized using three parameters: Strouhal number (St), maximum angle of attack $(\alpha_{\max})$, and heave amplitude to chord ratio. The corresponding parameters in rolling and pitching motion for a flapping foil are the St and $\alpha_{\max}$, as calculated at a location 70% of the distance from the root of the foil to the tip. The distance to this point from the axis of roll rotation is denoted by $r_{0.7}$. (Note that $r_{0.7} \geq 0.7s$ where s is the span of the foil.) The ratio of the arc length at $r_{0.7}$ to the chord, denoted as $h_{0.7}/c$, replaces the heave amplitude to chord ratio from the two-dimensional (2-D) case.

Now, for three-dimensional (3-D) kinematics, we can express the angle of attack at $r_{0.7}$ as

$$\alpha(t) = -\arctan\left(\frac{\omega r_{0.7} \phi_0 \cos(\omega t)}{U}\right) + \theta_0 \cos(\omega t) + \theta_{\text{bias}}. \tag{4}$$

For 3-D kinematics, the Strouhal number is defined as

$$St = \frac{2 r_{0.7} \phi_0 f}{U}. \tag{5}$$

The Strouhal number can be thought of as a measure of the aggressiveness of the flapping motion with respect to the incoming flow speed. Maintaining the same St while increasing the flow speed requires an increase in flapping frequency, amplitude, or both. The factor of two results in scaling as a function of approximate wake width, which emphasizes the relationship between St and vortex shedding patterns in the foil wake.
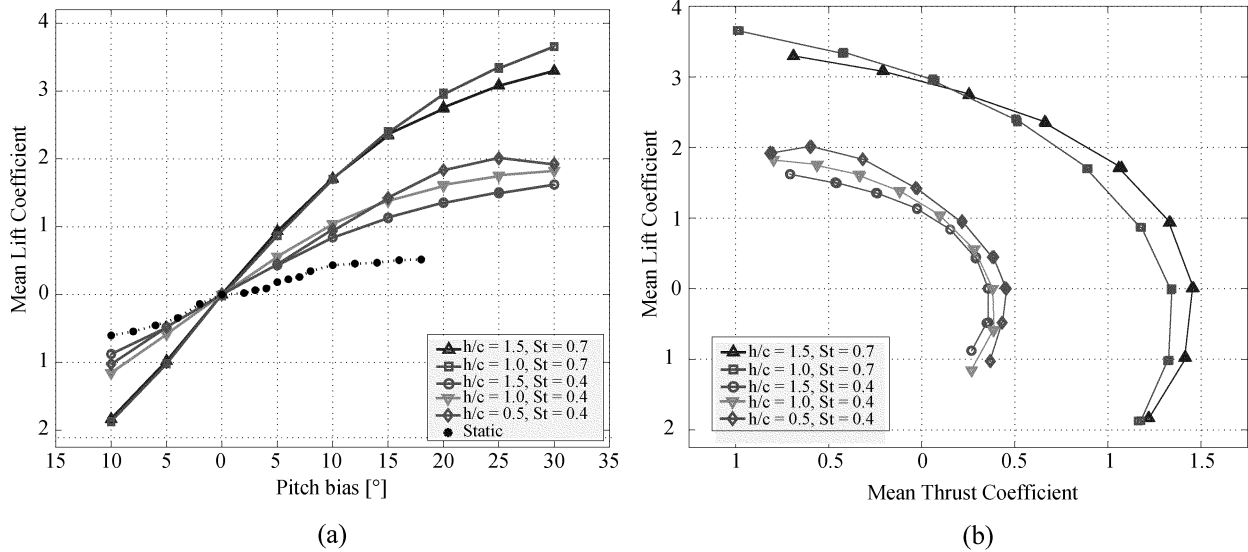
Fig. 4. Effect of pitch bias on C_L and C_T. (a) Mean C_T versus pitch bias θ_{bias}. (b) Mean C_L versus C_T.

B. Water Tunnel Test Results

The prototype of the initial foil module design module was mounted under a six-axis dynamometer in the MIT water tunnel. Details of the tunnel actuator construction and experimental apparatus can be found in [11].

Along with extensive testing of pure thrust producing modes across a range of St number and α_{max} with flow speeds between 0.4 and 1.0 m/s, the production of maneuvering forces, i.e., forces perpendicular to the fluid flow, was investigated. The maneuvering forces were generated by adding constant bias θ_{bias} to the foil pitch angle throughout the entire propulsive stroke.

The experiments were performed at five points in the sample space of Strouhal number and α_{max}, where relatively high thrust coefficients were observed. Bias angles from $-10°$ up to $40°$ in $5°$ increments were tested at St of 0.4 and 0.7 and $h_{0.7}/c$ values of 1.0 and 1.5. Bias angles from $-10°$ up to $30°$ were tested at $St = 0.4$ and $(h_{0.7}/c) = 0.5$. α_{max} for all tests was held at $40°$. Nondimensional lift and thrust coefficients C_L and C_T were calculated as

$$C_T = \frac{T}{\frac{1}{2}\rho U^2 A_{\text{foil}}} \qquad (6)$$

$$C_L = \frac{L}{\frac{1}{2}\rho U^2 A_{\text{foil}}} \qquad (7)$$

where T and L are the thrust and lift force, ρ is the fluid density, U is the flow velocity, and A_{foil} is the foil area.

In each case, as shown in Fig. 4(a), this relatively simple pitch bias strategy results in a near-linear relationship between lift coefficient and bias angle. A similar relationship is also found in experiments with heaving and pitching foils in the MIT testing tank [10]. Much higher lift coefficients are available in this manner than with the foil acting as a traditional, nonflapping, or static control surface, with mean lift coefficients over 3 recorded in two cases, at θ_{bias} of $25°$ and $30°$, in contrast to a maximum lift coefficient of 0.5 before stall for the static foil.
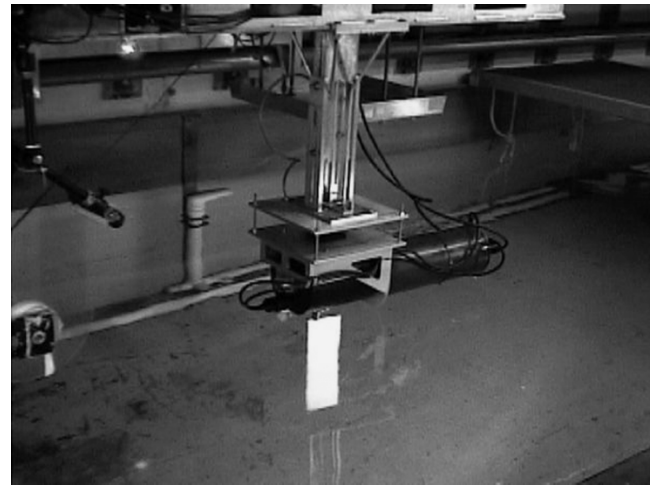

Fig. 5. Towtank actuator test apparatus.

Fig. 4(b) plots the lift coefficient against the thrust coefficient for each of the five sets of kinematics. The effect of higher amplitudes is seen to be much less significant than the Strouhal number in determining the location and shape of the curve. Note that maximum angle of attack is held constant throughout. For a more detailed discussion of the tests, including flow visualization results, see [11].

C. Testing Tank Results

One of the four actuators constructed for use on the vehicle was mounted to the Model Testing Tank towing carriage below a two-axis dynamometer with the foil submerged (Fig. 5). Testing was performed across a four-dimensional (4-D) test matrix, varying St, α_{max}, ϕ_o, and foil aspect ratio. All of the towed experiments were performed at a towing velocity of 0.5 m/s. Details of the experimental apparatus and the complete experimental results can be found in [12].

Fig. 6 consists of plots of C_T developed as a function of the nondimensional parameters at three different values of ϕ_o to
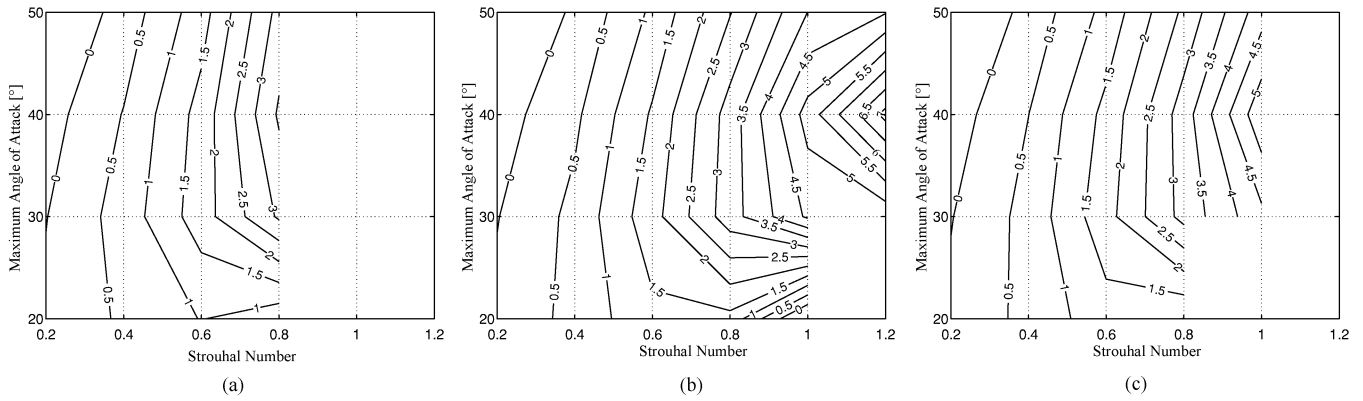
Fig. 6.　Contours of thrust coefficient, roll angle ($20°$ $40°$, $60°$). (a) $20°$ roll amplitude; (b) $40°$ roll amplitude; (c) $60°$ roll amplitude.

demonstrate the insensitivity of the developed thrust coefficient to the amplitude of the roll motion at any given Strouhal number and $\alpha_{\max}$. The plots represent data from experiments using a foil with a span of 40 cm and constant chord of 10 cm, with roll angles of $20°$, $40°$, and $60°$. There is little to distinguish between the results other than the increased operational range of the actuator, in terms of the nondimensional coefficients, when the roll amplitude is increased to $60°$. Note that for the $60°$ roll angle, thrust coefficients between 0 and 7 are available to the actuator.

V. VEHICLE PERFORMANCE AND CONTROL

A. Projected Vehicle-Cruising Performance

The data in this paper is presented in normalized form, which tends to hide practical effect of the limits of the actuator mechanism on the foil performance. We would like to extrapolate the experimental results to higher speeds in order to make predictions about vehicle performance limits, specifically speed limits, with this actuator design. Several assumptions allow us to do so, as follows.

- Distance r_{eff} from the roll axis to the effective center of force on the foil is solely a function of Strouhal number and $\alpha_{\max}$.
- Maximum lift is generated at the maximum roll angular velocity (which coincides with zero roll angular acceleration).
- Maximum roll motor torque coincides either with maximum lift or maximum foil acceleration.
- Effective added mass of water in rotation about the roll axis is always much smaller than the rotational inertia of the moving parts of the actuator.

Previous tests have confirmed that these are a realistic, if not comprehensive, set of assumptions. Under these assumptions, the question of whether the vehicle can operate up to some speed can be answered by answering two separate questions.

- First, can the foil actuator motors supply the power needed to overcome the water resistance at the moment of maximum foil angular rotation?

    Motor output power requirements peak at the coincidence of maximum foil angular rotation and maximum foil

lift. The relations for torque and for speed at this moment, in terms of the kinematics and measured lift coefficients, are

$$\tau_{\max} = L_{\max} r_{\text{eff}} \tag{8}$$
$$\dot{\phi}_{\max} = \phi_\circ \omega. \tag{9}$$

To extrapolate from known data points, we can maintain St and $\alpha_{\max}$ so that, by the assumptions above, r_{eff} is constant. Hence, the roll motor torque requirement at the moment of maximum lift scales with U^2

$$L_{\max} = \frac{1}{2}\rho U^2 A_{\text{foil}} C_{L\max} \sim U^2. \tag{10}$$

From (5), we see that shaft speed scales with flow velocity as well if St is held constant

$$\phi_\circ \omega = \frac{U \cdot St}{r_{0.7}\pi} \sim U. \tag{11}$$

Since output power for the motor is calculated as

$$P = \tau\omega \sim U^3 \tag{12}$$

it follows that power output required at the moment of maximum lift scales with the flow velocity cubed (when St and $\alpha_{\max}$ are held constant).

- Second, can the motors supply the zero-speed torque required to overcome the rotational inertia of the foil apparatus at the moment of maximum foil angular acceleration?

    Foil roll axis angular acceleration and maximum angular acceleration are given by

$$\ddot{\phi} = -\phi_\circ \omega^2 \sin \omega t \tag{13}$$
$$|\ddot{\phi}_{\max}| = \phi_\circ \omega^2. \tag{14}$$

Discounting the added mass of the fluid, we find that the torque required to overcome the rotational inertia in the roll scales linearly with the roll amplitude and with the square of the frequency.

The discussion of actuator limits here has focused on the roll actuation, as it is clear from experiments with the current design that the pitch motor is overpowered with respect to the roll motor for the simple harmonic kinematics described above.
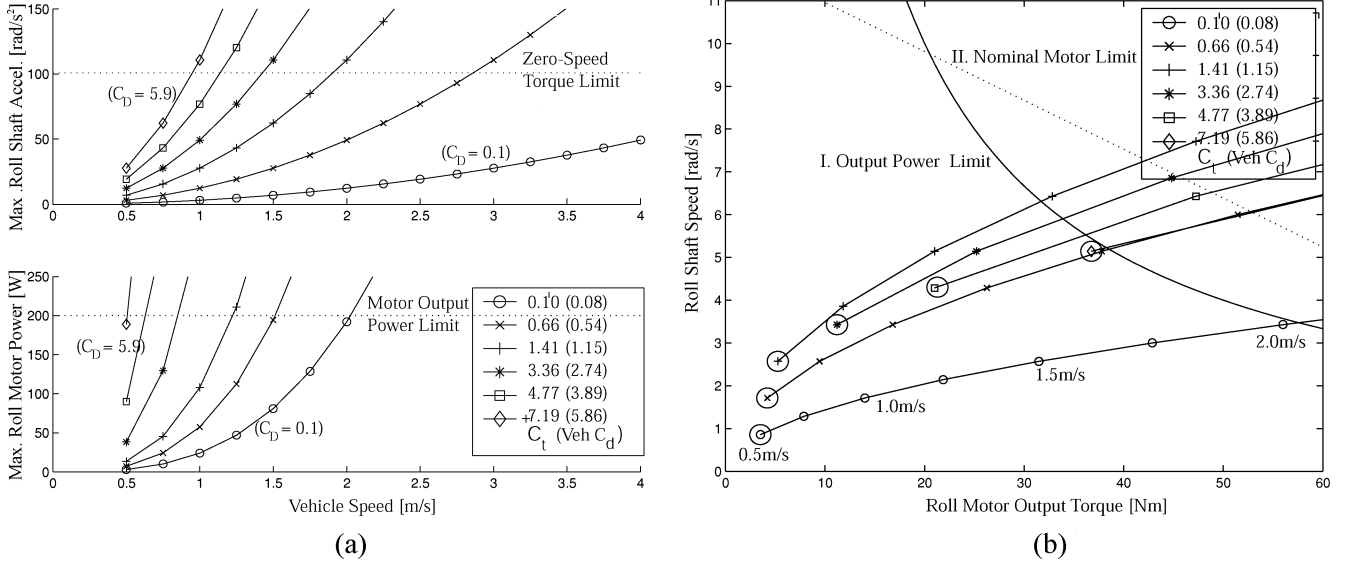
Fig. 7. Estimation of vehicle cruising speed limits for varying C_D, with four 0.40 m × 0.10 m foils). (a) Output power and foil roll acceleration limits. (b) Roll motor torque-speed requirements with flow-speed increase.

It is now possible to make a quantitative estimate of the actual velocity limit for a vehicle using four of the existing foil modules, with 0.40 m × 0.10 m foils. In both configurations described previously, all four foils are oriented with the foil thrust direction directly forward in the vehicle body frame. Defining a drag coefficient for the vehicle based on the vehicle projected frontal area $C_D = \left(D/((1/2)\rho U^2 A_{\text{vehicle}})\right)$, the equation for the total thrust force required of the foils is

$$T_{\text{tot}} = C_T \cdot \left(\frac{1}{2}\rho U^2\right) \cdot A_{\text{foils}} \tag{15}$$

$$= C_D \cdot \left(\frac{1}{2}\rho U^2\right) \cdot A_{\text{vehicle}} \tag{16}$$

$$\text{or} \quad C_T = C_D \frac{A_{\text{vehicle}}}{A_{\text{foils}}}. \tag{17}$$

The maximum speed of the vehicle, as a function of the drag coefficient of the vehicle, is the maximum speed at which a foil actuator can produce the required C_T.

For the following analysis, power and acceleration requirements are extrapolated from six data points, representing six different sets of foil kinematics tested at a flow speed of 0.5 m/s. These kinematics are considered to be desirable because of their relatively low maximum current draw as a function of thrust coefficient, as experimentally demonstrated in the Towing Tank. The foil thrust coefficients range from 0.10 to 7.19. For a ratio of foil area to vehicle frontal area of 0.8, these values correspond to vehicle drag coefficients of 0.08–5.86.

Fig. 7(a) shows how the power and zero-speed torque limits of the actuator roll motor limit the maximum speed of the vehicle. As the vehicle speed increases (from left to right on the horizontal axis), the corresponding power and torque required are shown to increase. For each set of kinematics, the motor limits are reached at some vehicle speed. The zeros-speed torque limit shown is a conservative value of 101 rad/s^2, which is based on the maximum acceleration achieved by the actuator during tests

with the 0.40 m foil in water. The motor power limit results from current limiting the roll motor amplifier to 12 A at 24 V, combined with and the manufacturer's estimate of 75% efficiency across the motor's two-stage planetary gear head. These figures indicate that regardless of the vehicle drag coefficient, the primary limitation on the vehicle maximum speed is the power required to drive the foil at maximum velocity.

For further visualization of the motor power limit, Fig. 7(b) shows the change in the motor operating point as vehicle speed increases. This plot indicates how the maximum power limit is approached for each of the six different thrust coefficients selected. Curve I represents maximum power output of 201 W, while curve II is the nominal motor torque-speed curve at 24 V. Each point to the right along a curve represents a vehicle-speed increase of 0.25 m/s, starting from a speed of 0.5 m/s. (The 0.5 m/s point is circled for each curve.)

For a streamlined vehicle, a drag coefficient of 0.1 is attainable with difficulty, which would yield a vehicle maximum speed of greater than 2 m/s. Without a streamlined fairing, a drag coefficient between 0.8 and 1.4 is more appropriate, from [13] based on the drag on a blunt cylinder with aspect ratio $(l/d) = 4$, indicating a maximum speed under 1 m/s.

Typical propeller-driven ocean-going AUVs, as detailed in [14], are operated at speeds between 0.7–2.5 m/s. The comparably sized MIT Sea Grant Odyssey class vehicles cruise at between 1.5–2 m/s. The REMUS vehicles from the Woods Hole Oceanographic Institution (WHOI), Woods Hole, MA, which have a frontal area of 0.029 m^2 and a measured drag coefficient as low as 0.267, can be operated at 1.5 m/s using around 20 W for propulsion [15]. The Autonomous Benthic Explorer (ABE), a 1200-lb AUV from the Deep Submergence Laboratory at WHOI is generally run at 0.7 m/s with an approximately 200-W mean propulsive power requirement [16]. While all three of these vehicles use elongated and streamlined body shapes in order to reduce drag and increase range, it should be noted that, at present, propeller-driven AUVs can achieve speeds in the

range postulated for the flapping foil vehicle with lower power consumption.

B. Control Considerations During Cruising Operation

Fig. 4(b) demonstrates that a foil should be able to generate maneuvering forces perpendicular to the vehicle motion while it is being used to propel the vehicle. The shape of the curves about the zero-mean lift point in each case indicates that for small bias angles (less than 5°), significant lift can be developed with a relatively slight drop in thrust. The weak coupling between thrust and lift generation for small pitch bias for a given operating point should allow for the decoupling of speed and pitch control in a vehicle being controlled to constant forward speed. In the fore–aft paired fin configuration, there is the option to use either one or both pairs of foils in concert to generate pitch moments. In the boxfish orientation, yaw can also be actuated by using pitch bias on the up–down oriented fins.

For speed control, accurate measurement of flow speed will be necessary to ensure that effective kinematics are chosen for the foils. Once a steady-state speed has been achieved, maintaining that speed may be as straightforward as a proportional-integral-derivative (PID) controller that varies the frequency of the foil motion, as the foil thrust coefficient generally is a strong function of Strouhal number at high $\alpha_{\max}$. In both speed and pitch control, some higher level decisions about the relative merits of adjusting frequency and amplitude to achieve the desired Strouhal number will need to be made as well. As demonstrated in Fig. 7(a), the rotational inertia of the apparatus does not limit the vehicle speed when using a consistent roll amplitude of 60° for cruising, indicating that lower roll amplitudes and higher frequency motions could be used to achieve the same total thrust.

The appeal of higher frequency motions is greater control bandwidth, assuming that the kinematics of the foil motion are adjusted only after complete swimming strokes. For example, reducing roll amplitude to 20° from 60° at a flow speed of 0.5 m/s, assuming a desired thrust coefficient of 1.4, would increase the flapping frequency from 0.3 to 1 Hz. Eventually, a frequency and amplitude combination would be reached, at which the rotational inertia of the actuator would effectively limit the motion.

C. Control Considerations During Hovering Operations

A tradeoff is also found between bandwidth and actuator authority when considering zero speed maneuvers, i.e., hovering. Fig. 8 qualitatively illustrates how the available actuator authority can decline with increasing frequencies, as explained later. The plot shows idealized contours of thrust as a function of foil oscillating frequency and roll amplitude. Overlaid on these contours are the various limits that come into play as frequency and/or amplitude increase.

Experiments with the foil actuator, operated in the towing tank with no forward speed, suggest that both mean thrust and maximum current draw are primarily functions of the maximum roll angular velocity. Fig. 9 shows contours of mean thrust, while Fig. 10 shows the corresponding contours of maximum current. All tests were performed using simple harmonic motion about the roll-and-pitch axes, with roll amplitudes from 20° to 60° and
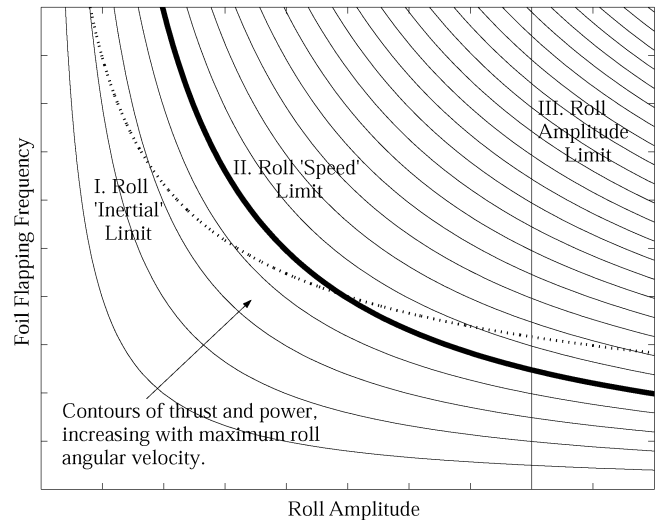

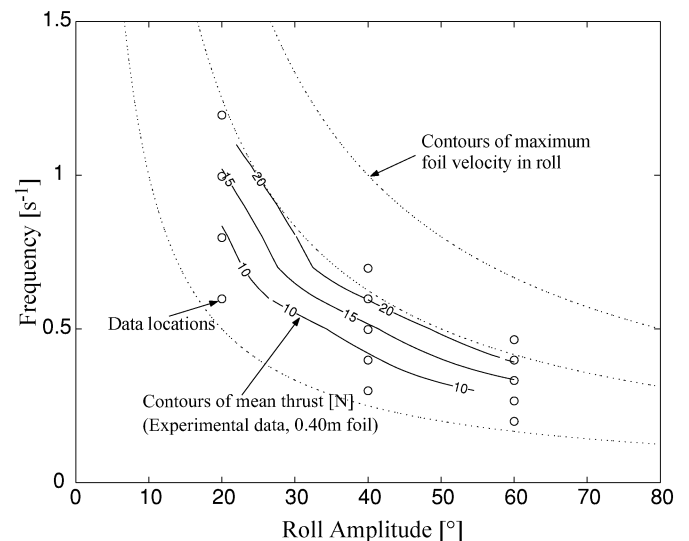Fig. 8.   Shape of actuator hovering limits.

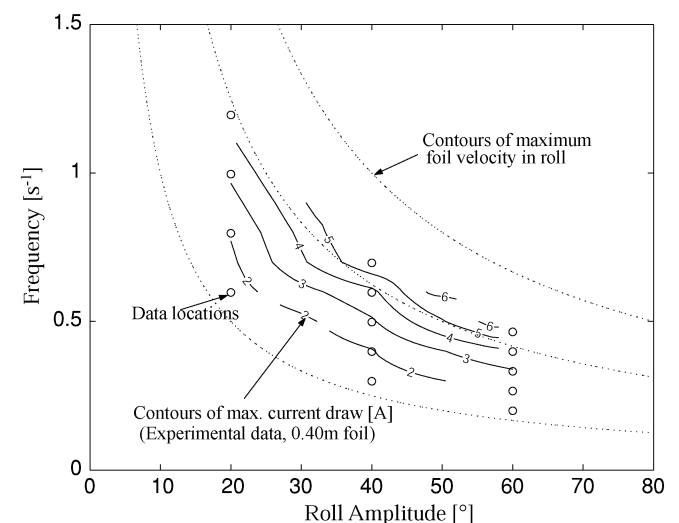Fig. 9.   Contours of mean thrust for 0.40-m foil in Hover.

Fig. 10.   Contours of maximum current draw for 0.40-m foil in hover.

a pitch amplitude of 60°. In each case, contours of maximum roll angular velocity are included to illustrate the correlation.

Curve I on Fig. 8 indicates the "inertial" limit that is imposed by the finite roll motor stall torque. The motor stall torque limits the maximum angular acceleration of the motor, which scales with $\phi_{\mathrm{o}}\omega^2$. Curve I is, thus, the shape of the contour line representing a single value of the motor stall torque—foil kinematics above and to the right of this line require a higher value of the stall torque.

Curve II indicates the roll motor power limit. The current to the roll motor is limited for safety purposes and since both maximum current draw and mean thrust are proportional to maximum angular velocity, a limit on the current must be represented by a line that follows a thrust contour. Foil kinematics above and to the right of curve II require a higher current limit.

Finally, Curve III indicates a hard physical limit on the roll amplitude ϕ_{o}, which is 90° for this actuator. Foil kinematics to the right of this line are physically impossible with the current actuator.

Thrust contours increase following the arrow from the bottom left to the top right, so a level of thrust can be achieved only if the corresponding contour at some point is to the left and below each of the limit curves. As the level of thrust of the contours increases up to curve II, the intersection with curve I, the "inertial" limit occurs at lower frequencies. Hence, as thrust is increased, the maximum frequency and, hence, the control bandwidth decreases.

VI. CONCLUSION

A design is detailed for a biomimetic flapping foil underwater vehicle. By focusing attention on the design of independently housed actuators, an easily reconfigurable vehicle was created. This configuration flexibility will allow the vehicle to be used as a platform for experimentation with different vehicle shapes, foil properties, and even varying numbers of foils.

Due to the unsteady nature of the foil actuation, evaluation of vehicle performance limits must focus on analysis of the maximum power output requirements for the actuators, which can be several times the mean. Estimates of the maximum cruising velocity of an underwater vehicle powered by four of the foils described above are found to be between 1 and 2 m/s. The result ultimately depends on the vehicle drag coefficient, which is assumed to be in the range from $C_D =0.1$ to 1.4. While comparably sized AUVs are capable of achieving these speeds with lower power consumption than the BFFAUV, there are many possible means for improvement of operating efficiency that have not yet been explored.

In addition to projecting the performance of the vehicle, issues of vehicle control using flapping foils were discussed. One promising point is the ability to generate maneuvering forces linearly proportional to an easily adjustable parameter, the foil pitch bias angle, without significantly degrading thrust. This linear relationship between bias angle and lift force is appealing, as it suggests that control strategies used with traditional control surfaces can be extended to include flapping foils.

At low vehicle speeds, a tradeoff is demonstrated between control bandwidth and actuator authority. There is a choice between large forces supplied by high-amplitude motions at low frequencies and smaller forces supplied by low-amplitude high-frequency motions.

REFERENCES

[1] F. Fish, "Power output and propulsive efficiency of swimming bottlenose dolphins," *J. Exp. Biol.*, vol. 185, pp. 179–193, 1993.
[2] G. Lauder and B. Jayne, "Speed effects on midline kinematics during steady undulatory swimming of largemouth bass," *J. Exp. Biol.*, vol. 198, pp. 585–602, 1995.
[3] J. Videler, *Fish Swimming*. London, U.K.: Chapman and Hall, 1992.
[4] M. Triantafyllou, D. Yue, S. Tolkoff, A. Techet, D. Barrett, F. Hover, M. Grosenbaugh, W. McGillis, and M. Wolfgang, "Drag reduction and turbulence control in swimming fish-like bodies," in *Proc. Int. Symp. Seawater Drag Reduction*, Newport, RI, July 1998, pp. 463–469.
[5] D. Barrett, M. Triantafyllou, M. G. D. Yue, and M. Wolfgang, "Drag reduction in fish-like locomotion," *J. Fluid Mech.*, vol. 392, pp. 183–212, 1999.
[6] N. Kato, "Control performance in horizontal plan of fish robot with mechanical pectoral fins," *IEEE J. Oceanic Eng.*, vol. 25, pp. 121–129, Jan. 2000.
[7] P. Bandyopadhyay, J. Castano, J. Rice, J. Phillips, R. Nedderman, and W. Macy, "Low speed maneuvering hydrodynamics of fish and small underwater vehicles," *J. Fluids Eng.*, vol. 119, pp. 136–144, 1997.
[8] J. Anderson, "Vorticity control for efficient propulsion," Ph.D. dissertation, Dept. Oceanographic Eng., Massachusetts Inst. Technol., Cambridge, Feb. 1996.
[9] D. Read, "Oscillating foils for propulsion and maneuvering of ships and underwater vehicles," M.S. thesis, Dept. Naval Architect. Marine Eng., Massachusetts Inst. Technol., Cambridge, Feb. 1999.
[10] O. Haugsdal, "Motion control of oscillating foils for steady propulsion and starting maneuvers," M.S. thesis, Massachusetts Inst. Technol., Cambridge, 2000.
[11] M. Flores, "Flapping motion of a three dimensional foil for propulsion and maneuvering of underwater vehicles," M.S. thesis, Dept. Ocean Eng., Massachusetts Inst. Technology, Cambridge, May 2003.
[12] V. Polidoro, "Flapping foil propulsion for cruising and hovering autonomous underwater vehicles," M.S. thesis, Dept. Ocean Eng., Massachusetts Inst. Technology, Cambridge, May 2003.
[13] S. Hoerner, "Fluid-Dynamic Drag," Hoerner Fluid Dynamics, Vancouver, WA, 1965.
[14] J. Yuh, "Design and control of autonomous underwater robots: A survey," *Int. J. Autonomous Robots*, vol. 8, pp. 7–24, 2000.
[15] B. Allen, W. S. Vorus, and T. Prestero, "Propulsion system performance enhancements on REMUS AUVs," in *Proc. IEEE OCEANS Conf. Rec.*, vol. 3, 2000, pp. 1869–1873.
[16] A. M. Bradley, M. D. Feezor, H. Signh, and F. Y. Sorrell, "Power systems for autonomous underwater vehicles," *IEEE J. Oceanic Eng.*, vol. 26, pp. 526–538, Oct. 2001.

Stephen Licht received the B.S. degree in mechanical engineering from Yale University, New Haven, CT, in 1998 and is currently working toward the Ph.D. degree in ocean engineering at the Massachusetts Institute of Technology, Cambridge/Woods Hole Oceanographic Institution, Woods Hole, MA, joint program.

Victor Polidoro received the B.S. degree in mechanical engineering from the University of Illinois, Urbana-Champaign, in 2000, and the M.S. degree in ocean engineering from the Massachusetts Institute of Technology (MIT), Cambridge, in 2003.

He currently is a Research Engineer with the Autonomous Underwater Vehicles Laboratory, MIT Sea Grant.

Melissa Flores received the B.S. and M.S. degrees in ocean engineering from the Massachusetts Institute of Technology (MIT), Cambridge, in 2002 and 2003, respectively.

She is currently serving as an Officer onboard the *USS Preble*, based out of San Diego, CA.

Franz S. Hover (A'93) received the B.S.M.E. degree from Ohio Northern University, Ada, in 1987 and the S.M. and Sc.D. degrees in oceanography/applied ocean science and engineering from the Massachusetts Institute of Technology (MIT), Cambridge/Woods Hole Oceanographic Institution, Woods Hole, MA, joint program in 1989 and 1993, respectively.

He was a Postdoctoral Fellow with the Monterey Bay Aquarium Research Institute, Monterey, CA, from 1994 to 1995. He joined MIT in 1997, where he has worked in the areas of nontraditional propulsion and maneuvering in marine vehicles and in vortex-induced vibrations. He has also been a regular Consultant to the military and to industry.

Michael S. Triantafyllou received the S.M. degree in ocean engineering and mechanical engineering and the Ph.D. degree in ocean engineering from the National Technical University of Athens, Greece, in 1977 and 1979, respectively.

He has been with the Ocean Engineering Department, Massachusetts Institute of Technology (MIT), Cambridge, since 1978, first as a Research Associate (from 1978 to 1979), then as an Assistant Professor (from 1979 to 1983), Associate Professor (from 1983 to 1990), and currently as a Professor, since 1990. He currently is the Director of the Testing Tank and Propeller Testing Facilities. His research is focused on vorticity control and flow-structure interaction, control of marine vehicles, and biomimetic propulsion and maneuvering.

Dr. Triantafyllou has received the following awards: Best Graduate Paper Award (SNAME) in 1978; the Doherty Professorship in Ocean Utilization from 1983 to 1985; the American Bureau of Shipping (ABS)/Linnard Prize for best paper (SNAME) in 1997; Highlight Paper of 1995 Scientific American; and the Discover Magazine Award for Technological Innovation in 1998.